Journal of Materials Chemistry A

ROYAL SOCIETY OF CHEMISTRY

PAPER

View Article Online
View Journal | View Issue

Cite this: J. Mater. Chem. A, 2024, 12, 21933

Addressing ambient stability challenges in pure $FASnI_3$ perovskite solar cells through organic additive engineering†

Sergio Galve-Lahoz,[ab] Jesús Sánchez-Diaz,[a] Carlos Echeverría-Arrondo,[ac] Jorge Simancas,[a] Jhonatan Rodriguez-Pereira,[de] Silver-Hamill Turren-Cruz,[af] Juan P. Martinez-Pastor,[f] Iván Mora-Seró *[a] and Juan Luis Delgado *[bg]

Tin halide perovskite solar cells (Sn-PSCs) have emerged as promising alternatives to their lead-based counterparts. However, their potential for commercialization is threatened by their inherent stability issues and lower efficiencies that have not yet matched those of established technologies. Therefore, in this work we strategically designed and synthesized two novel organic compounds, referred to as **OM4** and **OM6**, which have been successfully incorporated as additives into pure $FASnI_3$ PSCs enhancing the crystal properties and simultaneously acting as protective and passivating agents. Through a systematic exploration of chemical interactions, **OM4** and **OM6** demonstrated a remarkable ability to improve film morphology and optical properties. Consequently, both additives significantly contributed to the enhancement of the overall device performances and exhibited impressive stabilities in the ambient atmosphere, which is attributed to their hydrophobic nature. Notably, the unencapsulated devices incorporating **OM4** and **OM6** retained over 80% and 90% of their initial power conversion efficiency (PCE) after 250 hours in the ambient atmosphere at RH = 30%, respectively; in contrast, the devices without any of the organic additives suffered complete degradation after 72 hours under the same conditions. As a result, this work opens new possibilities in the rational design and development of organic additives capable of mitigating the instability and low-performance issues commonly associated with Sn-PSCs.

Received 11th May 2024
Accepted 10th July 2024

DOI: 10.1039/d4ta03291h

rsc.li/materials-a

Introduction

Lead-based perovskite solar cells (Pb-PSCs) have demonstrated great potential to surpass well-established silicon-based solar cells and enter into the photovoltaic market, showing a huge increase in power conversion efficiency (PCE) from the first reported 3.8% in 2009 (ref. 1) to the recently certified >26%.[2,3] However, despite their outstanding properties,[4–7] the presence of toxic lead (Pb^{2+})[8,9] in these devices hinders their universal commercialization.[10,11] To address this issue, researchers have been exploring alternative divalent cations, including germanium (Ge^{2+}),[12,13] copper (Cu^{2+})[14] and tin (Sn^{2+}).[15–17] Among them, tin has recently emerged as one of the most promising candidates to replace lead in perovskite solar cells due to their chemical similarities.[18,19]

Owing to their close location in the periodic table within the same group, both tin and lead share analogous electronic configurations and atomic sizes (1.49 Å for Pb^{2+} and 1.35 Å for Sn^{2+}),[20] resulting in comparable behaviors as metal cations within perovskite solar cells. In fact, tin-based halide perovskite solar cells (Sn-PSCs) have also demonstrated exceptional properties, including high carrier mobilities,[21] high absorption coefficients in the visible region,[22] long exciton lifetimes,[23] and suitable optimal band gaps within the range of 1.2–1.4 eV.[24,25] Furthermore, Sn-based perovskites exhibit a higher level of environmental compatibility than Pb-based perovskites.[26] This is primarily attributed to the tendency of the byproducts generated during the degradation of Sn-based perovskites to undergo hydrolysis in water forming SnI_4, SnO_2, and A_2SnI_4 (A

[a]Institute of Advanced Materials (INAM), University Jaume I, Av. Vicent Sos Baynat, s/n, 12071, Castellón de la Plana, Spain. E-mail: sero@uji.es
[b]Polymat, University of the Basque Country UPV/EHU, 20018 Donostia-San Sebastian, Spain. E-mail: juanluis.delgado@polymat.eu
[c]Institute of Chemical Research of Catalonia (ICIQ), Avda. Països Catalans 16, 43007 Tarragona, Spain
[d]Center of Materials and Nanotechnologies, Faculty of Chemical Technology, University of Pardubice, nám. Cs. legií 565, Pardubice, 53002, Czech Republic
[e]Central European Institute of Technology, Brno University of Technology, Purkynova 123, Brno, 61200, Czech Republic
[f]Instituto de Ciencia de los Materiales (ICMUV), Universitat de Valencia, 46980 Paterna, Spain
[g]Ikerbasque, Basque Foundation for Science, Bilbao 48013, Spain

† Electronic supplementary information (ESI) available. See DOI: https://doi.org/10.1039/d4ta03291h

= methylammonium or formamidinium),[27–29] which exhibit lower solubility in water compared to the byproducts derived from Pb-based perovskites, and make Sn-PSCs more suitable candidates for future commercial applications.[30]

Nevertheless, Sn^{2+} presents higher Lewis acidity in comparison to its Pb^{2+} counterpart.[31] This disparity in acidity results in accelerated reactions between the perovskite precursors, typically SnI_2 and FAI, leading to rapid and uncontrolled crystallization processes.[32,33] Consequently, non-homogeneous films with pinhole-rich structures and a high density of defects are usually obtained. It has been widely reported that structural defects may promote the adsorption of water and oxygen molecules onto the perovskite layer, thereby accelerating the degradation process and affecting the stability and operational performance of the final solar cell devices.[34,35] Moreover, structural defects can act as non-radiative recombination centers, leading to losses in open-circuit voltage (V_{OC}), which significantly limit the overall performance of the solar cell devices. In this sense, finding new compounds capable of effectively interacting with Sn-PSC precursors to improve the crystallization process and simultaneously passivate the defects formed through the perovskite matrix is essential to obtain high-quality Sn-PSCs.

Another drawback associated with Sn-PSCs is their inherent instability upon exposure to the ambient atmosphere, resulting in fast degradation and significant drops in the device performance. This instability mainly arises from the tendency of Sn^{2+} to oxidize, in the presence of water or oxygen molecules, to the more stable Sn^{4+} state.[36–38] Subsequently, the proliferation of Sn^{2+} vacancies within the perovskite lattice gives rise to a detrimental p-type self-doping phenomenon, which can lead to an alteration in the charge transport properties and overall electrical characteristics of the Sn-PSCs, resulting in considerable V_{OC} losses.[39,40] To overcome this issue, several approaches have been explored, including effective surface passivation,[41–44] the introduction of different reducing agents,[45–47] or the formation of stable 2D/3D perovskites, among other methods.[48–50] Another interesting methodology widely explored in Pb-PSCs but barely applied to Sn-PSCs to efficiently enhance their stability in air involves the incorporation of hydrophobic compounds, which successfully confer a protective effect on the devices against deleterious external factors.[51–54]

With these facts in mind, in this work we strategically designed two novel organic additives, namely **OM4** and **OM6**, each possessing two external acrylate moieties attached to the central structures to allow partial polymerization processes. Acrylates are a type of vinyl monomer that can undergo polymerization at moderate temperatures through a process known as thermal polymerization.[55–58] This method can take advantage of the intrinsic annealing step necessary for the correct perovskite crystallization process, without the need for additional steps such as UV-light treatments that may damage the perovskite film.[59–61] Additionally, **OM4** and **OM6** were designed with distinct cores to explore the role of different functional groups as additives in Sn-PSCs. As such, **OM4** features a pyridine functional group (Lewis base-type), already reported in Sn-PSCs,[33,62] whereas **OM6** includes a less explored 1,2,4,5-tetrafluorobenzene unit (Lewis acid-type).

After the introduction of the additives into the Sn perovskite films, a significant enhancement in the PCE of the Sn-PSCs was observed. The initial PCE of 7.78% for the pristine $FASnI_3$ (FA, formamidinium) increased to 9.18% and 9.62% upon the addition of **OM4** and **OM6**, respectively. More interestingly, the treated devices displayed exceptional stability after more than 250 h of storage under ambient conditions (at a relative humidity of 30% and a temperature of 25 °C), retaining up to 80% and 90% of their initial PCE for **OM4** and **OM6** treated devices, respectively. In contrast, pristine $FASnI_3$ devices completely degraded after only 72 h of storage under the same conditions.

Results and discussion

Both **OM4** and **OM6** were synthesized following the synthetic routes described in Schemes S1 and S2, respectively, in the ESI,† and their chemical structure is illustrated in Fig. 1a and b. More information about the synthetic and characterization details can be found in the ESI (see Fig. S1–S17†).

With the aim of understanding the role of the additives in the perovskite film morphology, we conducted scanning electron microscopy (SEM) measurements. Fig. 1c–e show the top-view SEM images of the $FASnI_3$ perovskite films with and without **OM4** and **OM6**. Note that additives were introduced in the perovskite layer during the antisolvent stage[63] solved in chlorobenzene (see the ESI† for further details). For clarity, the Sn-based perovskite films treated with **OM4** and **OM6** will be referred to as **Sn-OM4** and **Sn-OM6**, respectively. In the case of pristine $FASnI_3$, the film exhibited a non-uniform, pinhole-rich morphology due to the rapid and uncontrolled crystallization process typically associated with Sn-based perovskites.[33,64] However, upon the incorporation of the different additives, higher quality films were obtained, and the presence of pinholes was significantly reduced in both scenarios. Specifically, **Sn-OM4** showed a more compact film with a considerably lower number of pinholes, although some morphological defects were still present. On the other hand, **Sn-OM6** exhibited an extremely compact layer with no pinholes and a slight increase in the grain size. To provide a broader perspective on the positive impact of these additives on the perovskite crystallization process, and to demonstrate that the enhancement of the film morphology is not a local coincidence, lower magnification SEM images were obtained and presented in Fig. S18.† However, from the SEM cross-sectional images, we can observe that the incorporation of the additives does not affect the thickness of the perovskite films, as all samples exhibited a similar thickness of around 200 nm (see Fig. S18†). To confirm the presence of the additives within the perovskite film, we carried out Fourier Transform Infrared Spectroscopy (FTIR) on the perovskite films with and without additives, as well as on the individual **OM4** and **OM6** molecules (see Fig. S19†). The characteristic carbonyl group peak around 1730 cm^{-1}, along with the additional peaks in the fingerprint region, confirms the presence of the additives in the **Sn-OM4**

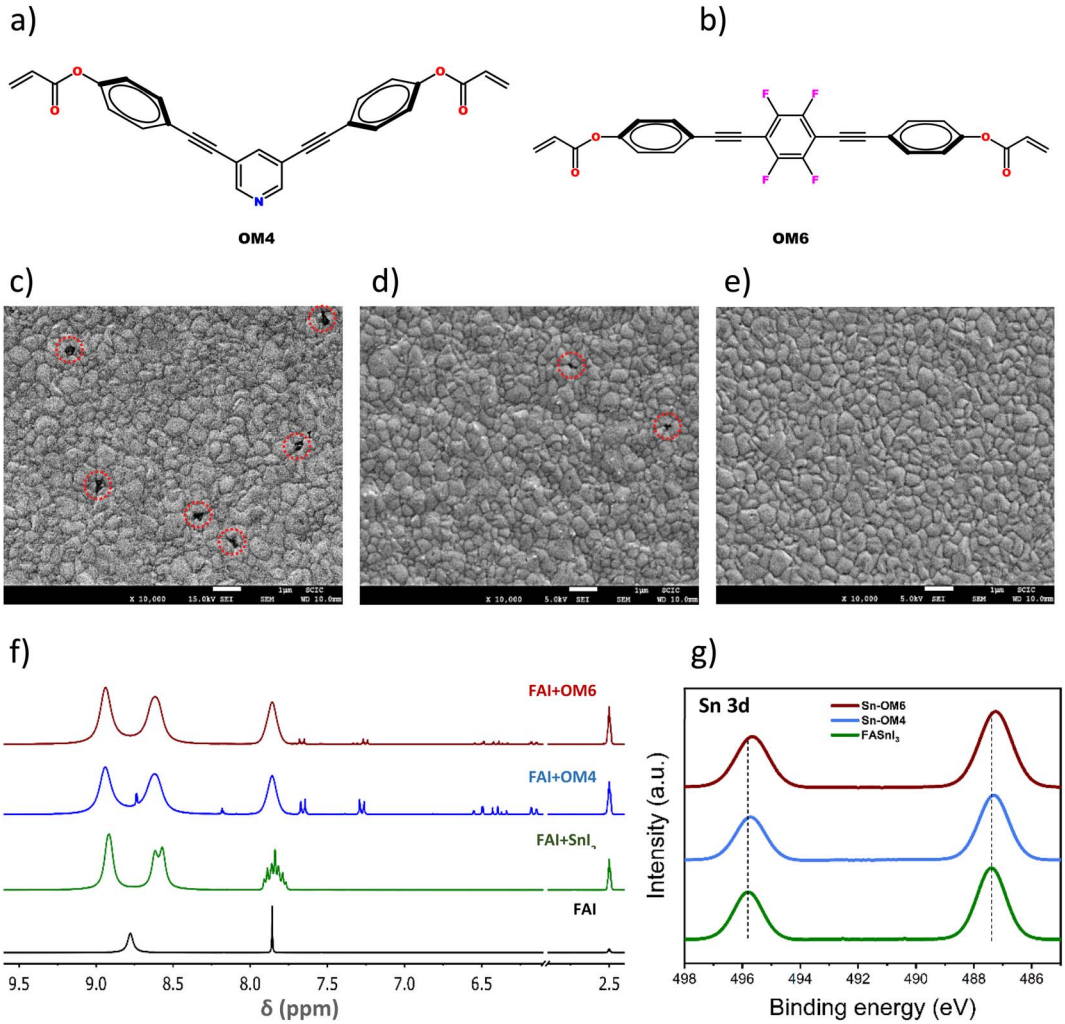

Fig. 1 Chemical structures of the (a) **OM4** and (b) **OM6** molecules. Top-view SEM images of (c) $FASnI_3$, (d) **Sn-OM4**, and (e) **Sn-OM6** films, some pinholes are highlighted with dotted red circles. (f) ^{1}H NMR spectra of FAI in DMSO-d_6 with and without SnI_2, **OM4** and **OM6**. (g) X-ray photoelectron spectroscopy spectra of Sn 3d for the perovskite films with and without **OM4** and **OM6**.

and **Sn-OM6** films. Additionally, the double peak observed around 1600 cm^{-1} in the **OM4** and **OM6** spectra corresponds to the $=CH_2$ double bonds present in the acrylate groups. Upon perovskite crystallization and thermal annealing, these peaks disappeared, indicating the polymerization of the materials. However, due to the limited sensitivity of the technique, we cannot entirely rule out the coexistence of single molecules and the polymerized materials in certain regions of the final perovskite film.

As previously noted, the rapid reaction between tin(II) iodide (SnI_2) and formamidinium iodide (FAI) often results in uncontrolled crystallization processes, yielding low-quality films characterized by random orientations and numerous defects such as pinholes and cracks.[65] Intermediate adducts formed between additives and SnI_2 or FAI precursors have been found to slow down reaction rates, thereby retarding the crystallization rate and leading to higher quality films.[33,38] For a better understanding of the role of **OM4** and **OM6** in the perovskite crystallization process, we conducted nuclear magnetic resonance (NMR) experiments. All NMR experiments were conducted in deuterated dimethyl sulfoxide-d_6 (DMSO-d_6) and referenced accordingly. To analyze the interactions with the perovskite precursors, we performed a combination of proton and fluorine nuclear magnetic resonance spectroscopies (^{1}H-NMR and ^{19}F-NMR) for different mixtures. Fig. 1f shows the ^{1}H NMR spectra of FAI, FAI + SnI_2, FAI + **OM4**, and FAI + **OM6**. In the FAI spectra, the proton peaks located around 7.8 and 8.8 ppm correspond to C–H and N–H protons, respectively. After the addition of SnI_2 to the FAI solution, the signal at 8.8 ppm splits into two distinct signals at 8.9 and 8.6 ppm, indicating a change in the charge distribution around N–H protons within the formamidinium group, possibly due to the formation of a hydrogen bond between the amidinium moiety and the SnI_2 species. Furthermore, a spiking in the signals at 7.8 and 8.6 is observed, which can be attributed to the presence of HI, likely formed as a consequence of the partial reaction of the SnI_2 species with traces of water present in the deuterated solution, as previously reported.[66] Interestingly, upon addition of **OM4**

and **OM6** to the FAI solution, the same splitting was observed, suggesting the formation of an adduct between FAI and **OM4** and **OM6** *via* hydrogen bonding.[67] Full range ^{1}H-NMR spectra showing all combinations are presented in Fig. S20 and S21.† To further understand the different behaviors of the pyridine and 1,2,4,5-tetrafluorobenzene units of **OM4** and **OM6**, we also conducted ^{1}H-NMR for **OM4** and ^{19}F-NMR for **OM6**, both with and without SnI_2, as depicted in Fig. S22 and S23.† In the case of **OM4**, two distinct proton signals were observed within the pyridine ring, located at chemical shifts of 8.77 and 8.19 ppm. Upon addition of SnI_2 to the deuterated solution, a noticeable downfield shift was observed in both signals, with a more remarkable shift observed in the signal corresponding to the proton adjacent to the nitrogen (N) atom. This shielding effect observed in the pyridine ring's protons suggests an electronic sharing between the lone pair of electrons present on the N atom and the vacant p orbital of the SnI_2 species, resulting in the formation of a Lewis acid–base adduct. Furthermore, peaks became narrower and more defined in the presence of SnI_2, indicative of greater molecular ordering. On the other hand, the role of the 1,2,4,5-tetrafluorobenzene unit present in **OM6** was studied *via* ^{19}F-NMR due to the absence of hydrogen atoms in the ring. Accordingly, the ^{19}F-NMR spectra of **OM6** with and without SnI_2 were obtained, and a clear upfield shift in the fluorine (F) signal was observed when SnI_2 was added, indicating a reduction in the electron density around the fluorinated ring. This spectral alteration also confirms an interaction wherein electronic density is shared between the electron-rich F atoms present in the 1,2,4,5-tetrafluorobenzene unit and the electronically deficient SnI_2 species. This phenomenon has been described before using fluorine-rich additives in lead-based PSCs.[68] These results point to the presence of interactions between the perovskite precursors and both **OM4** and **OM6**, which in turn modulate the crystallization kinetics, ultimately improving the film quality in the perovskite active layer, as previously observed in the SEM images.

In order to explore the chemical bonding properties of the different $FASnI_3$ perovskite films, with and without additives, X-ray photoelectron spectroscopy (XPS) analysis was employed (see Fig. 1g). As reported elsewhere, the characteristic XPS Sn^{2+} $3d_{5/2}$ peak that corresponds to the $FASnI_3$ perovskite was observed at 487.39 eV.[69] Interestingly, with the incorporation of **OM4** and **OM6**, this peak exhibited a small shift towards 487.31 eV and 487.25 eV, respectively. The shift of a specific element in its binding energy peak position typically reflects alterations in its local chemical environment, indicating a variation in the electron density surrounding the nucleus.[15,70,71] The contrast between the reference films and the **OM4** or **OM6** treated films suggests an elevated level of coordination with the 3d orbitals of Sn^{2+} when **OM4** or **OM6** is introduced; however, it should be noted that the incorporation of **OM6** leads to superior coordination. This observation clarifies the improved crystallization properties observed in the presence of **OM6** compared to **OM4** and $FASnI_3$ without any additive.

Additionally, to evaluate the role of the organic additives in the inhibition of the oxidation of Sn^{2+} into Sn^{4+}, the Sn $3d_{5/2}$ and $3d_{3/2}$ XPS spectra of the $FASnI_3$, **Sn-OM4** and **Sn-OM6** films were recorded, depicted in Fig. S24.† All the peak binding energies of Sn^{2+} and Sn^{4+} are summarized in Table S1†. The Sn^{4+} content was quantified, revealing a higher value for the pristine $FASnI_3$ film (5,9%) compared to the **Sn-OM4** (4.3%) and **Sn-OM6** (3.7%) films (see Fig. S25†). These results are in perfect agreement with the expected role of the additives as crystal regulators.

To obtain more information on the impact of the additives on the crystallographic properties of the perovskite films, we performed X-ray diffraction (XRD) analysis. Fig. 2a shows the XRD patterns of the $FASnI_3$ films with and without **OM4** and **OM6**. The addition of additives did not alter the crystal structure of the $FASnI_3$ perovskite film, and in all cases, the XRD patterns exhibited the typical peaks corresponding to the orthorhombic lattice. Concretely, six different diffraction peaks appear at angle values of 14.1°, 24.5°, 28.2°, 31.7°, 37.5°, and 50.5°, which can be ascribed to the (100), (120), (200), (211), (222), and (300) planes, respectively.[72] In both **Sn-OM4** and **Sn-OM6** films, a preferred crystal orientation in the (100) plane was observed as can be inferred from the increase in the relative intensity of the peaks corresponding to this plane.[73] Moreover, a clear reduction in the Full Width at Half-Maximum (FWHM) of the (100) and (120) diffraction peaks was noted, indicating a larger crystalline size particularly evident when **OM6** was present (see Fig. S26†). Furthermore, it is evident that the addition of **OM4** and **OM6** does not induce any significant shift in the different diffraction peaks, suggesting that neither of the additives were incorporated into the perovskite crystalline lattice. Instead, they might be located at grain boundaries and crystal surfaces acting as passivating agents.

To investigate the effect of the additives on the optical properties and gain insights into their role in the perovskite film, we conducted ultraviolet-visible absorption (UV-vis), steady-state photoluminescence (PL), and time-resolved PL spectroscopy (TRPL) measurements. Fig. 2b shows the UV-vis absorption spectra. The films treated with **OM4** and **OM6** showed slightly superior light absorption properties compared to pristine $FASnI_3$ films. This behavior is in good agreement with the morphological results and is attributed to the formation of larger grain domains and the reduced presence of pinholes or cracks in the perovskite film.[74] Furthermore, we performed PL and TRPL measurements to study the charge dynamics in the presence of **OM4** and **OM6** (see Fig. 2c and d respectively). The PL spectrum is shown in Fig. 2c. No significant shift in the bandgap was detected; however, the treated perovskite films exhibited a notorious increase in PL intensity in comparison with the control film, indicating a reduction in the effective non-radiative trap-assisted recombination. Given that the absorption coefficient in Sn-based perovskites can be in the order of 4×10^4 cm^{-1}, and the thickness of the film is around 200 nm, carriers are uniformly photogenerated throughout the whole film thickness, hence trap states located at the grain boundaries can be the dominant non-radiative channels, over those located at the perovskite surface. The TRPL spectra (see Fig. 2d) were fitted with a biexponential decay function using the following equation:

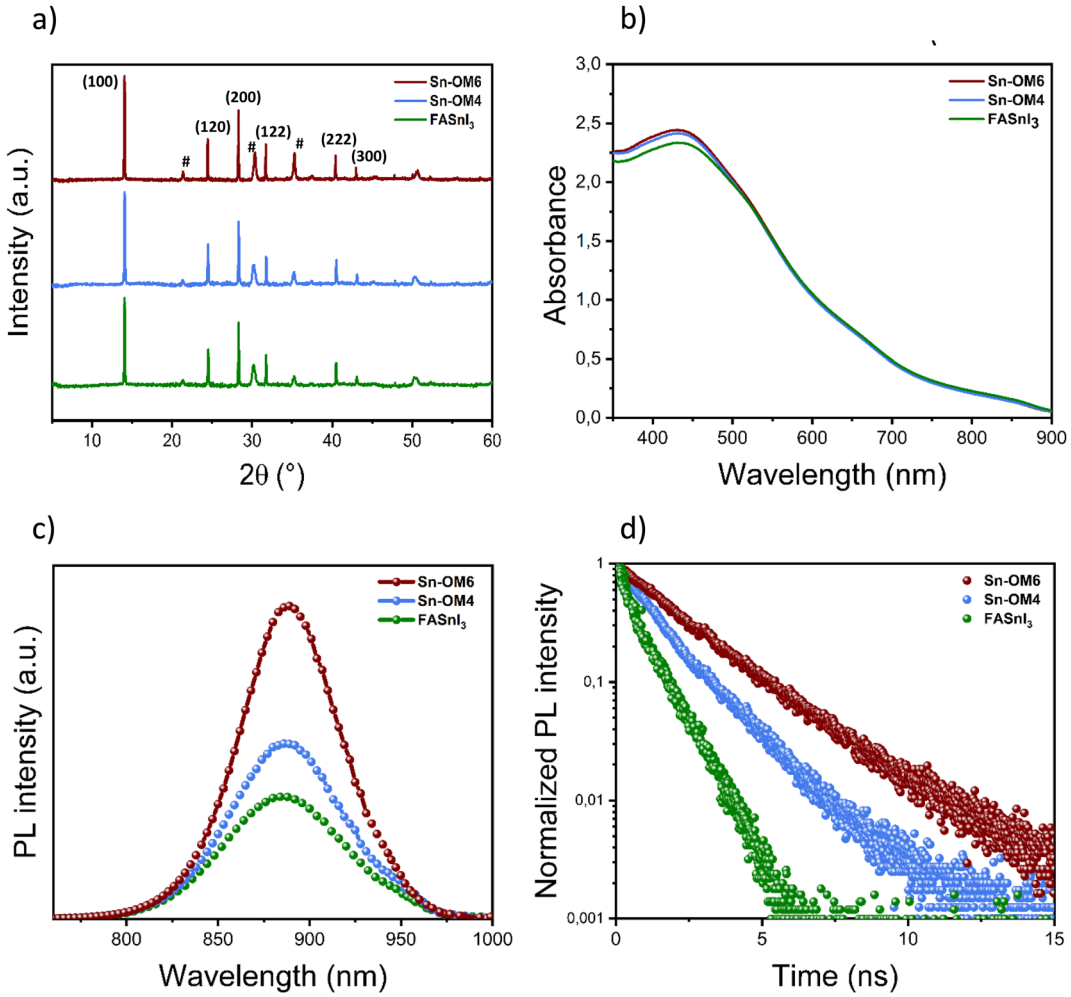

Fig. 2 Structural and optical characterization of $FASnI_3$ films prepared with and without **OM4** and **OM6** and deposited on glass substrates. (a) X-ray diffraction patterns for different perovskite films; # indicates the diffraction peaks corresponding to ITO. (b) UV-vis absorption spectrum for $FASnI_3$ films prepared with and without additives. (c) PL spectra and (d) time-resolved PL decays corresponding to $FASnI_3$ with and without additives.

$$\tau_{ave} = \frac{(A_1\tau_1 + A_2\tau_2)}{(A_1 + A_2)} \quad (1)$$

where τ_1 stands for the fast decay component and τ_2 for the slow decay component, as also observed in other lead-free materials.[75] The best fitting parameters are listed in Table S2.† τ_1 was prolonged from 0.4 ns ($FASnI_3$) to 1.3 ns (**Sn-OM4**) and 2.0 ns (**Sn-OM6**). Taking into account the large inhomogeneities in the Sn-based perovskite films, as reflected by the high full width at half maximum of PL spectra in Fig. 2c, this component can be related to localized and/or free excitons whose decay time would be $1/\tau_1 = 1/\tau_{Xr} + 1/\tau_{nr}$, where τ_{Xr} would be the excitation radiative lifetime and τ_{nr} the non-radiative trap-assisted recombination time. The observed increase in τ_1 confirms the reduction of non-radiative recombination centers. On the other hand, τ_2 could be tentatively associated with bimolecular (band-to-band) radiative recombination and is also limited by the same non-radiative channels, and hence the observed elongation: **Sn-OM6** (3.5 ns) > **Sn-OM4** (2.8 ns) > $FASnI_3$ (1.1 ns) (see Table S2†) confirms again the improved quality of the films when the additives are added.[76]

Additionally, we analyzed the changes in the relative positions of the energy bands and determined the cut-off for the valence band maximums, which is represented in Fig. S27.† As shown in Fig. 2b and c, the bandgap remained unchanged. Therefore, a slightly lower valence band could result in a lower conduction band position, correcting the misalignment specially for **Sn-OM4** and **Sn-OM6** with the C60 ETL, which is one of the main reasons behind the lower V_{OC} in Sn-based perovskite solar cells.

This systematic characterization highlights the beneficial role of **OM4** and **OM6** additives in the properties of $FASnI_3$ films. On one hand, they modulate the crystallization kinetics and improve the film quality. On the other hand, XPS characterization reveals a reduction in Sn^{4+} content, and optoelectronic characterization demonstrates a reduced non-radiative recombination. Since XRD spectra do not show a change in the lattice parameters, we propose that additives may be located at perovskite grain boundaries, suppressing the detrimental non-radiative recombination typical of these defect-rich domains. This behavior suggests a superior performance of

Sn-PSCs with light harvesting Sn-perovskite films containing **OM4** and **OM6** additives.

To validate this potentiality, we evaluated the role of the additives in Sn-PSC performance. Solar cell devices were fabricated adopting an inverted p–i–n configuration that consisted of ITO/PEDOT:PSS/$FASnI_3$/C_{60}/BCP/Ag, as shown in Fig. 3a. As a first step, the concentration for both additives was optimized to 0.40 mM (see Fig. S28 and 29†). The current density–voltage (*J*–*V*) curves for the best-performing PSCs in each system are depicted in Fig. 3b and Table S3.† Their corresponding photovoltaic parameters, including V_{OC}, short-circuit current-density (J_{SC}), fill factor (FF) and PCE are summarized in Fig. 3c–f and Table S4.† It is important to note that all the devices underwent a light soaking treatment at 1 sun irradiance in a N_2 atmosphere. This post-treatment procedure is incorporated as part of a routine purification process to mitigate the amount of Sn^{4+} states within the perovskite active layer, as previously demonstrated by our group.[45] The control devices showed a maximum efficiency of 7.71% with a J_{SC} of 19.91 mA cm^{-2}, a V_{OC} of 0.581 V, and an FF of 66.59%. The **OM4** treated champion device displayed an improved efficiency of 9.25% with a similar J_{SC} of 19.97 mA cm^{-2}, a significantly improved V_{OC} of 0.689 V and an FF of 67.14%. The **OM6** treated champion device showed the maximum efficiency of 9.66%, with a similar J_{SC} of 20.04 mA cm^{-2}, a greatly increased V_{OC} of 0.706 V and a slightly increased FF of 68.23%. It is worth mentioning that the photocurrent obtained from the integration of the external quantum efficiency (EQE) is in good agreement with the one obtained from the *J*–*V* measurements (see Fig. S30†). The enhancement of the device performance is mainly attributed to the higher V_{OC} presented by the Sn-PSCs treated with the additives. Concretely, the average V_{OC} (see Table S4†) increased from 0.57 V for the pristine $FASnI_3$ perovskite to 0.67 V and 0.71 V for the devices treated with **OM4** and **OM6**, respectively, and consequently resulted in a significant average PCE enhancement of 25% and 37%, respectively. This improvement in V_{OC}, and ultimately in PCE, can be attributed to a reduced carrier recombination within **Sn-OM4** and **Sn-OM6** perovskite layers. This effect, at the same time, may be ascribed to the formation of more compact and pinhole-free perovskite layers, along with the passivation of the remaining defects present in the matrix,[77] as already discussed after the characterization of perovskite layers. Moreover, control devices showed higher hysteresis behavior, which is suppressed upon the additive treatments, as shown in Fig. S31.† This can be linked to a lower trap density, which retards the ion migration across the perovskite film.[78] Notably, it is also important to highlight the increase in reproducibility with the use of the additives, especially **OM6**, as Fig. S32† shows. This better reproducibility can be attributed to the enhanced pinhole-free morphology of **Sn-OM6** films (see Fig. 1e).

Moreover, to better understand the role of defects and additives in the improved performance of our solar cells, we investigated $FASnI_3$ surfaces with adsorbed **OM4** and **OM6** molecules by density functional theory (DFT) simulations. The atomic structures of the input surfaces and output densities of states (DOS) are given in Fig. S33 and S34,† respectively. The DOS (Fig. S34†) include the contribution from N atoms in **OM4** molecules and from F atoms in **OM6** molecules. Interestingly, the projected DOS reflect a contribution from N atomic orbitals to the conduction band minima which is missing, indeed, for F

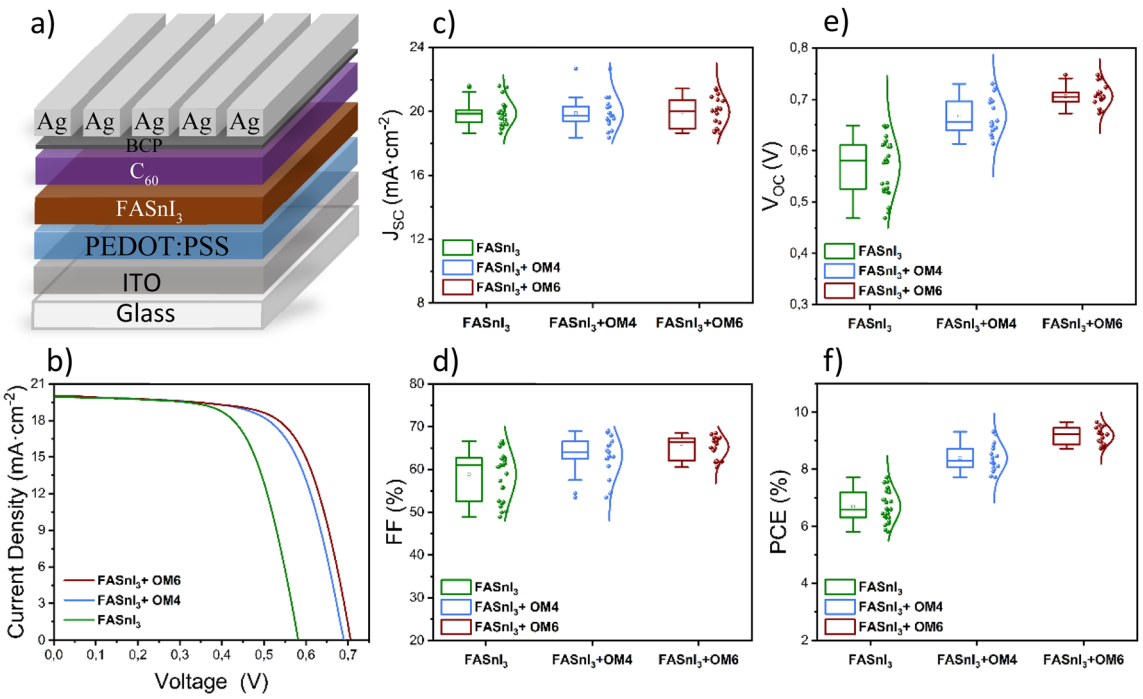

Fig. 3 (a) Sn-PSC device architecture, (b) best performing devices' *J*–*V* curves, (c–f) statistics of the solar cell parameters: (c) J_{SC}, (d) FF, (e) V_{OC} and (f) PCE. All the parameters were extracted from *J*–*V* curves under 100 mW cm^{-2} AM 1.5G illumination.

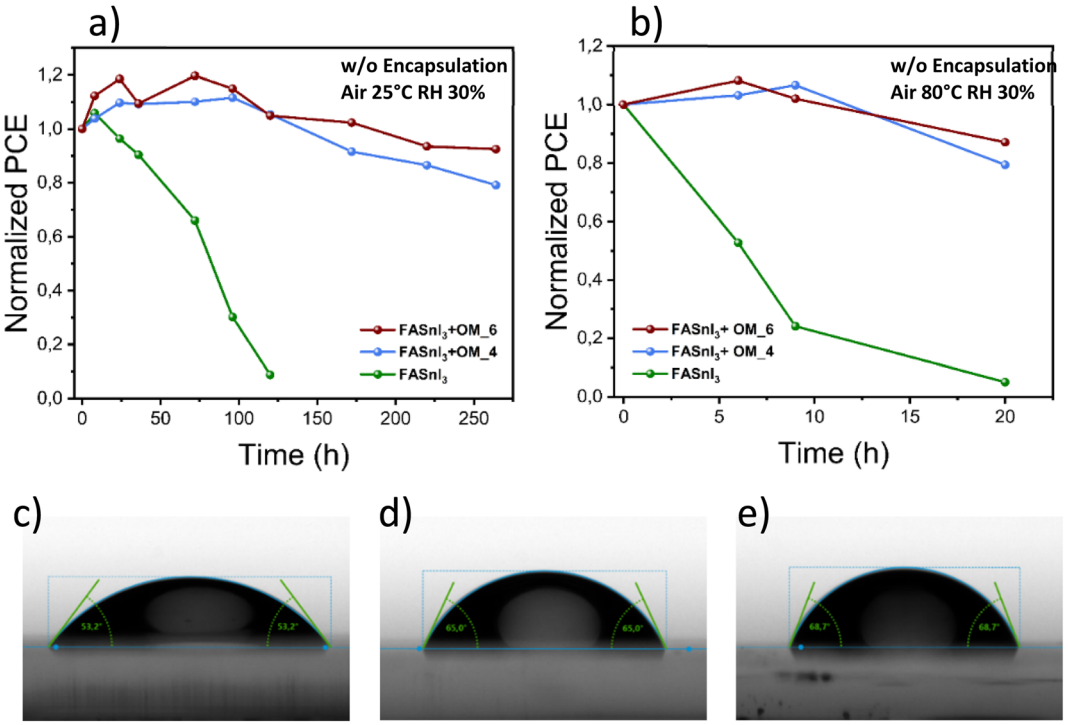

Fig. 4 PCE evolution of unencapsulated devices with and without OM4 or OM6 stored in (a) air at RH = 30% and 25 °C and (b) at RH = 30% and 80 °C. Contact angle of water droplets on the surface of (c) pristine $FASnI_3$, (d) **Sn-OM4** and (e) **Sn-OM6**.

atoms. The strong localization of photocarriers at N sites can be considered as a plausible reason behind the lower average improvement of solar cell performance reached with the **OM4** additive.

Finally, even more significant than the effect of the additives in the PCE for Sn-PSCs are the implications in the device long-term stability. Sn-PSCs have demonstrated a very good stability under nitrogen conditions,[45] but a poor stability under ambient conditions. Consequently, in order to evaluate the stability of our devices under high stress conditions, we carried out shelf-stability tests in an oxygen atmosphere under normal conditions and under thermal stress. All the devices were tested without any encapsulation. Shelf-stability tests were carried out at RH = 30% and 25 °C. After 24 hours, control devices only retained 80% of their initial power conversion efficiency and completely degraded after just 72 hours. On the other hand, **OM4** treated devices maintained 80% of their initial PCE for 220 h. More impressively, **OM6** treated devices retained over 90% of their initial PCE for more than 250 h, which is among the highest air stabilities reported for pure 3D-phase $FASnI_3$ perovskites (see Fig. 4a and Table S5†). Additionally, we also kept track of the stability of the unencapsulated devices at 80 °C in air and a complete degradation of the control devices was observed after less than 10 h, while the devices containing **OM4** or **OM6** retained more than 85% of their initial PCE after more than 20 h (see Fig. 4b). This outstanding stability, here reported, is attributed to the high hydrophobicity of the additives, and their intrinsic and widely reported polymerization ability,[55–58] which act as protective barriers impeding water molecules from permeating and degrading the perovskite active layer. Also, the presence of hydrophobic aromatic rings within their structure, and additional fluorine atoms in the case of **OM6**, make both of them exceptional barriers to physically but not electronically isolate the perovskite layer. As shown in Fig. 4c–e, the enhanced hydrophobicity of the Sn-based perovskite films when **OM4** or **OM6** is present was demonstrated by performing water contact angle measurements. It can be observed that the contact angle of water drops over the pristine $FASnI_3$ film increased from 53.2° to 65.0° and 68.7° when **OM4** or **OM6** was added, respectively. As expected, the hydrophobicity of the **Sn-OM6** film was higher compared to that of **Sn-OM4** due to the presence of the well-known highly hydrophobic 1,2,4,5-tetrafluorobenzene unit.[79,80]

Conclusions

In summary, we developed and synthesized two novel organic additives containing different functional groups – a pyridine unit (**OM4**) and a 1,2,4,5-tetrafluorobenzene unit (**OM6**)-, which were incorporated into Sn-based perovskite solar cells as additives. Although both additives showed positive effects in the final performance of the devices, our findings indicated that the fluorinated ring located in **OM6** exhibits stronger coordination with the tin perovskite precursors compared to the more widely used pyridine unit (**OM4**), resulting in enhanced structural, optical and morphological properties. Consequently, a significant improvement in the performance of the solar cell devices was observed; in particular, the average PCE was increased 25% and 37%, with respect to the average PCE of the $FASnI_3$ control

cell, when **OM4** or **OM6** was incorporated as an additive, respectively.

Moreover, due to the highly hydrophobic nature of the organic additives, and likely their polymerization capabilities, a notorious enhancement in the stability of the devices was observed. Notably, even under ambient conditions without any encapsulation, the devices containing **OM4** and **OM6** preserved up to 80% and 90% of their initial PCE, respectively, for over 250 hours, whereas the pristine $FASnI_3$ devices suffered a complete degradation after 72 hours under the same conditions. Hence, this study contributes to the understanding of the role of different functional groups present in organic additives commonly utilized in tin perovskite solar cells, thereby paving the way for future rational molecular design of additives in this field. The additive inclusion strategy is shown to be a successful approach to bypass the limitations of PCE and long-term stability of Sn-PSCs.

Data availability

Data for this article are available at zenodo repository at **https://doi.org/10.5281/zenodo.12733691**.

Conflicts of interest

There are no conflicts to declare.

Acknowledgements

This work was partially funded by the Generalitat Valenciana *via* European Union-NextGeneration EU project Print-P (MFA/2022/020). S. H. T. C. gratefully acknowledges funding from the Ministry of Science and Innovation of Spain under Ayudas Ramón y Cajal (RYC2022-035578-I) for financial assistance during this work. J. R. P. acknowledges the Ministry of Education, Youth and Sports of the Czech Republic, for the financial support of XPS measurements using the CEMNAT infrastructure (project LM 2023037). J. L. D. acknowledges Ikerbasque, Basque Foundation for Science, for an "Ikerbasque Research Associate" contract, the Polymat Foundation, and the Spanish Government (PID2021-129084OB-I00 and RED2022-134344-T grants).

References

1 A. Kojima, K. Teshima, Y. Shirai and T. Miyasaka, Organometal Halide Perovskites as Visible-Light Sensitizers for Photovoltaic Cells, *J. Am. Chem. Soc.*, 2009, **131**(17), 6050–6051.
2 J. Park, J. Kim, H.-S. Yun, M. J. Paik, E. Noh, H. J. Mun, M. G. Kim, T. J. Shin and S. I. Seok, Controlled growth of perovskite layers with volatile alkylammonium chlorides, *Nature*, 2023, **616**(7958), 724–730.
3 **https://www.nrel.gov/pv/assets/pdfs/best-research-cell-efficiencies.pdf**.
4 H. S. Jung and N.-G. Park, Perovskite Solar Cells: From Materials to Devices, *Small*, 2015, **11**(1), 10–25.
5 J. Y. Kim, J.-W. Lee, H. S. Jung, H. Shin and N.-G. Park, High-Efficiency Perovskite Solar Cells, *Chem. Rev.*, 2020, **120**(15), 7867–7918.
6 J. Jeong, M. Kim, J. Seo, H. Lu, P. Ahlawat, A. Mishra, Y. Yang, M. A. Hope, F. T. Eickemeyer, M. Kim, Y. J. Yoon, I. W. Choi, B. P. Darwich, S. J. Choi, Y. Jo, J. H. Lee, B. Walker, S. M. Zakeeruddin, L. Emsley, U. Rothlisberger, A. Hagfeldt, D. S. Kim, M. Grätzel and J. Y. Kim, Pseudo-halide anion engineering for α-FAPbI3 perovskite solar cells, *Nature*, 2021, **592**(7854), 381–385.
7 S. Collavini, S. F. Völker and J. L. Delgado, Understanding the Outstanding Power Conversion Efficiency of Perovskite-Based Solar, *Cells*, 2015, **54**(34), 9757–9759.
8 A. Demayo, M. C. Taylor, K. W. Taylor, P. V. Hodson and P. B. Hammond, Toxic effects of lead and lead compounds on human health, aquatic life, wildlife plants, and livestock, *CRC Crit. Rev. Environ. Control*, 1982, **12**(4), 257–305.
9 G. Li, Y.-T. Liu, F. Yang, M. Li, Z. Zhang, J. Pascual, Z.-K. Wang, S.-Z. Wei, X.-Y. Zhao, H.-R. Liu, J.-B. Zhao, C.-T. Lin, J.-M. Li, Z. Li, A. Abate and I. Cantone, Biotoxicity of Halide Perovskites in Mice, *Adv. Mater.*, 2024, **36**(2), 2306860.
10 N. Moody, S. Sesena, D. W. deQuilettes, B. D. Dou, R. Swartwout, J. T. Buchman, A. Johnson, U. Eze, R. Brenes, M. Johnston, C. L. Haynes, V. Bulović and M. G. Bawendi, Assessing the Regulatory Requirements of Lead-Based Perovskite Photovoltaics, *Joule*, 2020, **4**(5), 970–974.
11 G. Schileo and G. Grancini, Lead or no lead? Availability, toxicity, sustainability and environmental impact of lead-free perovskite solar cells, *J. Mater. Chem. C*, 2021, **9**(1), 67–76.
12 I. Kopacic, B. Friesenbichler, S. F. Hoefler, B. Kunert, H. Plank, T. Rath and G. Trimmel, Enhanced Performance of Germanium Halide Perovskite Solar Cells through Compositional Engineering, *ACS Appl. Energy Mater.*, 2018, **1**(2), 343–347.
13 T. Krishnamoorthy, H. Ding, C. Yan, W. L. Leong, T. Baikie, Z. Zhang, M. Sherburne, S. Li, M. Asta, N. Mathews and S. G. Mhaisalkar, Lead-free germanium iodide perovskite materials for photovoltaic applications, *J. Mater. Chem. A*, 2015, **3**(47), 23829–23832.
14 W. Hu, X. He, Z. Fang, W. Lian, Y. Shang, X. Li, W. Zhou, M. Zhang, T. Chen, Y. Lu, L. Zhang, L. Ding and S. Yang, Bulk heterojunction gifts bismuth-based lead-free perovskite solar cells with record efficiency, *Nano Energy*, 2020, **68**, 104362.
15 J. Chen, J. Luo, E. Hou, P. Song, Y. Li, C. Sun, W. Feng, S. Cheng, H. Zhang, L. Xie, C. Tian and Z. Wei, Efficient tin-based perovskite solar cells with trans-isomeric fulleropyrrolidine additives, *Nat. Photonics*, 2024, **18**, 464–470.
16 S. Shao, J. Liu, G. Portale, H.-H. Fang, G. R. Blake, G. H. ten Brink, L. J. A. Koster and M. A. Loi, Highly Reproducible Sn-Based Hybrid Perovskite Solar Cells with 9% Efficiency, *Adv. Energy Mater.*, 2018, **8**(4), 1702019.

17 Z. Chen, J. J. Wang, Y. Ren, C. Yu and K. Shum, Schottky solar cells based on CsSnI3 thin-films, *Appl. Phys. Lett.*, 2012, **101**(9), 093901.

18 J. Seo, T. Song, S. Rasool, S. Park and J. Y. Kim, An Overview of Lead, Tin, and Mixed Tin–Lead-Based ABI3 Perovskite Solar Cells, *Adv. Energy Sustainability Res.*, 2023, **4**(5), 2200160.

19 A. Filippetti, S. Kahmann, C. Caddeo, A. Mattoni, M. Saba, A. Bosin and M. A. Loi, Fundamentals of tin iodide perovskites: a promising route to highly efficient, lead-free solar cells, *J. Mater. Chem. A*, 2021, **9**(19), 11812–11826.

20 R. Shannon, Revised effective ionic radii and systematic studies of interatomic distances in halides and chalcogenides, *Acta Crystallogr., Sect. A*, 1976, **32**(5), 751–767.

21 L. M. Herz, Charge-Carrier Mobilities in Metal Halide Perovskites: Fundamental Mechanisms and Limits, *ACS Energy Lett.*, 2017, **2**(7), 1539–1548.

22 N. K. Noel, S. D. Stranks, A. Abate, C. Wehrenfennig, S. Guarnera, A.-A. Haghighirad, A. Sadhanala, G. E. Eperon, S. K. Pathak, M. B. Johnston, A. Petrozza, L. M. Herz and H. J. Snaith, Lead-free organic–inorganic tin halide perovskites for photovoltaic applications, *Energy Environ. Sci.*, 2014, **7**(9), 3061–3068.

23 H.-H. Fang, S. Adjokatse, S. Shao, J. Even and M. A. Loi, Long-lived hot-carrier light emission and large blue shift in formamidinium tin triiodide perovskites, *Nat. Commun.*, 2018, **9**(1), 243.

24 W. Shockley and H. J. Queisser, Detailed Balance Limit of Efficiency of p-n Junction Solar Cells, *J. Appl. Phys.*, 1961, **32**(3), 510–519.

25 S. Rühle, Tabulated values of the Shockley–Queisser limit for single junction solar cells, *Sol. Energy*, 2016, **130**, 139–147.

26 C. Ponti, G. Nasti, D. Di Girolamo, I. Cantone, F. A. Alharthi and A. Abate, Environmental lead exposure from halide perovskites in solar cells, *Trends Ecol. Evol.*, 2022, **37**(4), 281–283.

27 L. Lanzetta, T. Webb, N. Zibouche, X. Liang, D. Ding, G. Min, R. J. E. Westbrook, B. Gaggio, T. J. Macdonald, M. S. Islam and S. A. Haque, Degradation mechanism of hybrid tin-based perovskite solar cells and the critical role of tin (IV) iodide, *Nat. Commun.*, 2021, **12**(1), 2853.

28 T. Leijtens, R. Prasanna, A. Gold-Parker, M. F. Toney and M. D. McGehee, Mechanism of Tin Oxidation and Stabilization by Lead Substitution in Tin Halide Perovskites, *ACS Energy Lett.*, 2017, **2**(9), 2159–2165.

29 D. J. Kubicki, D. Prochowicz, E. Salager, A. Rakhmatullin, C. P. Grey, L. Emsley and S. D. Stranks, Local Structure and Dynamics in Methylammonium, Formamidinium, and Cesium Tin(II) Mixed-Halide Perovskites from 119Sn Solid-State NMR, *J. Am. Chem. Soc.*, 2020, **142**(17), 7813–7826.

30 J. Li, H.-L. Cao, W.-B. Jiao, Q. Wang, M. Wei, I. Cantone, J. Lü and A. Abate, Biological impact of lead from halide perovskites reveals the risk of introducing a safe threshold, *Nat. Commun.*, 2020, **11**(1), 310.

31 X. Liu, T. Wu, X. Luo, H. Wang, M. Furue, T. Bessho, Y. Zhang, J. Nakazaki, H. Segawa and L. Han, Lead-Free Perovskite Solar Cells with Over 10% Efficiency and Size 1 cm2 Enabled by Solvent–Crystallization Regulation in a Two-Step Deposition Method, *ACS Energy Lett.*, 2022, **7**(1), 425–431.

32 F. Hao, C. C. Stoumpos, P. Guo, N. Zhou, T. J. Marks, R. P. H. Chang and M. G. Kanatzidis, Solvent-Mediated Crystallization of CH3NH3SnI3 Films for Heterojunction Depleted Perovskite Solar Cells, *J. Am. Chem. Soc.*, 2015, **137**(35), 11445–11452.

33 G. Nasti, M. H. Aldamasy, M. A. Flatken, P. Musto, P. Matczak, A. Dallmann, A. Hoell, A. Musiienko, H. Hempel, E. Aktas, D. Di Girolamo, J. Pascual, G. Li, M. Li, L. V. Mercaldo, P. D. Veneri and A. Abate, Pyridine Controlled Tin Perovskite Crystallization, *ACS Energy Lett.*, 2022, **7**(10), 3197–3203.

34 J. Hidalgo, W. Kaiser, Y. An, R. Li, Z. Oh, A.-F. Castro-Méndez, D. K. LaFollette, S. Kim, B. Lai, J. Breternitz, S. Schorr, C. A. R. Perini, E. Mosconi, F. De Angelis and J.-P. Correa-Baena, Synergistic Role of Water and Oxygen Leads to Degradation in Formamidinium-Based Halide Perovskites, *J. Am. Chem. Soc.*, 2023, **145**(45), 24549–24557.

35 G. Xie, L. Xu, L. Sun, Y. Xiong, P. Wu and B. Hu, Insight into the reaction mechanism of water, oxygen and nitrogen molecules on a tin iodine perovskite surface, *J. Mater. Chem. A*, 2019, **7**(10), 5779–5793.

36 Z. Zhang, Y. Huang, J. Jin, Y. Jiang, Y. Xu, J. Zhu and D. Zhao, Mechanistic Understanding of Oxidation of Tin-based Perovskite Solar Cells and Mitigation Strategies, *Angew. Chem., Int. Ed.*, 2023, **62**(45), e202308093.

37 L. Lanzetta, N. Aristidou and S. A. Haque, Stability of Lead and Tin Halide Perovskites: The Link between Defects and Degradation, *J. Phys. Chem. Lett.*, 2020, **11**(2), 574–585.

38 J. Pascual, G. Nasti, M. H. Aldamasy, J. A. Smith, M. Flatken, N. Phung, D. Di Girolamo, S.-H. Turren-Cruz, M. Li, A. Dallmann, R. Avolio and A. Abate, Origin of Sn(ii) oxidation in tin halide perovskites, *Adv. Mater.*, 2020, **1**(5), 1066–1070.

39 W. Ke, C. C. Stoumpos and M. G. Kanatzidis, "Unleaded" Perovskites: Status Quo and Future Prospects of Tin-Based Perovskite Solar Cells, *Adv. Mater.*, 2019, **31**(47), 1803230.

40 C. C. Stoumpos, C. D. Malliakas and M. G. Kanatzidis, Semiconducting Tin and Lead Iodide Perovskites with Organic Cations: Phase Transitions, High Mobilities, and Near-Infrared Photoluminescent Properties, *Inorg. Chem.*, 2013, **52**(15), 9019–9038.

41 E. Jokar, C.-H. Chien, A. Fathi, M. Rameez, Y.-H. Chang and E. W.-G. Diau, Slow surface passivation and crystal relaxation with additives to improve device performance and durability for tin-based perovskite solar cells, *Energy Environ. Sci.*, 2018, **11**(9), 2353–2362.

42 S. Hu, P. Zhao, K. Nakano, R. D. J. Oliver, J. Pascual, J. A. Smith, T. Yamada, M. A. Truong, R. Murdey, N. Shioya, T. Hasegawa, M. Ehara, M. B. Johnston, K. Tajima, Y. Kanemitsu, H. J. Snaith and A. Wakamiya, Synergistic Surface Modification of Tin–Lead Perovskite Solar Cells, *Adv. Mater.*, 2023, **35**(9), 2208320.

43 H. Yan, B. Wang, X. Yan, Q. Guan, H. Chen, Z. Shu, D. Wen and Y. Cai, Efficient passivation of surface defects by lewis

base in lead-free tin-based perovskite solar cells, *Mater. Today Energy*, 2022, **27**, 101038.
44 Y. Shi, Z. Zhu, D. Miao, Y. Ding and Q. Mi, Interfacial Dipoles Boost Open-Circuit Voltage of Tin Halide Perovskite Solar Cells, *ACS Energy Lett.*, 2024, 1895–1897.
45 J. Sanchez-Diaz, R. S. Sánchez, S. Masi, M. Krecmarová, A. O. Alvarez, E. M. Barea, J. Rodriguez-Romero, V. S. Chirvony, J. F. Sánchez-Royo, J. P. Martinez-Pastor and I. Mora-Seró, Tin perovskite solar cells with >1,300 h of operational stability in N2 through a synergistic chemical engineering approach, *Joule*, 2022, **6**(4), 861–883.
46 T. Wang, Q. Tai, X. Guo, J. Cao, C.-K. Liu, N. Wang, D. Shen, Y. Zhu, C.-S. Lee and F. Yan, Highly Air-Stable Tin-Based Perovskite Solar Cells through Grain-Surface Protection by Gallic Acid, *ACS Energy Lett.*, 2020, **5**(6), 1741–1749.
47 F. Hu, C.-H. Chen, Y.-H. Lou, T.-Y. Teng, Y.-R. Shi, Y. Xia, K.-L. Wang, J. Chen, Z.-K. Wang and L.-S. Liao, A vertical antioxidant strategy for high performance wide band gap tin perovskite photovoltaics, *J. Mater. Chem. A*, 2023, **11**(9), 4579–4586.
48 F. Wang, X. Jiang, H. Chen, Y. Shang, H. Liu, J. Wei, W. Zhou, H. He, W. Liu and Z. J. J. Ning, 2D-quasi-2D-3D hierarchy structure for tin perovskite solar cells with enhanced efficiency and stability, *Joule*, 2018, **2**(12), 2732–2743.
49 M. Li, W.-W. Zuo, Y.-G. Yang, M. H. Aldamasy, Q. Wang, S. H. T. Cruz, S.-L. Feng, M. Saliba, Z.-K. Wang and A. Abate, Tin Halide Perovskite Films Made of Highly Oriented 2D Crystals Enable More Efficient and Stable Lead-free Perovskite Solar Cells, *ACS Energy Lett.*, 2020, **5**(6), 1923–1929.
50 B.-B. Yu, Z. Chen, Y. Zhu, Y. Wang, B. Han, G. Chen, X. Zhang, Z. Du and Z. He, Heterogeneous 2D/3D Tin-Halides Perovskite Solar Cells with Certified Conversion Efficiency Breaking 14%, *Adv. Mater.*, 2021, **33**(36), 2102055.
51 S. Collavini, M. Saliba, W. R. Tress, P. J. Holzhey, S. F. Völker, K. Domanski, S. H. Turren-Cruz, A. Ummadisingu, S. M. Zakeeruddin, A. Hagfeldt, M. Grätzel and J. L. Delgado, Poly(ethylene glycol)–[60]Fullerene-Based Materials for Perovskite Solar Cells with Improved Moisture Resistance and Reduced Hysteresis, *ChemSusChem*, 2018, **11**(6), 1032–1039.
52 T.-H. Han, J.-W. Lee, C. Choi, S. Tan, C. Lee, Y. Zhao, Z. Dai, N. De Marco, S.-J. Lee, S.-H. Bae, Y. Yuan, H. M. Lee, Y. Huang and Y. Yang, Perovskite-polymer composite cross-linker approach for highly-stable and efficient perovskite solar cells, *Nat. Commun.*, 2019, **10**(1), 520.
53 S. Collavini, A. Cabrera-Espinoza and J. L. Delgado, Organic Polymers as Additives in Perovskite Solar Cells, *Macromolecules*, 2021, **54**(12), 5451–5463.
54 H. Uceta, A. Cabrera-Espinoza, M. Barrejón, J. G. Sánchez, E. Gutierrez-Fernandez, I. Kosta, J. Martín, S. Collavini, E. Martínez-Ferrero, F. Langa and J. L. Delgado, p-Type Functionalized Carbon Nanohorns and Nanotubes in Perovskite Solar Cells, *ACS Appl. Mater. Interfaces*, 2023, **15**(38), 45212–45228.
55 K. Miyazaki and T. Horibe, Polymerization of multifunctional methacrylates and acrylates, *J. Biomed. Mater. Res.*, 1988, **22**(11), 1011–1022.
56 Z. Zhu, D. Zhao, C.-C. Chueh, X. Shi, Z. Li and A. K. Y. Jen, Highly Efficient and Stable Perovskite Solar Cells Enabled by All-Crosslinked Charge-Transporting Layers, *Joule*, 2018, **2**(1), 168–183.
57 Z. Liu, F. Liu, C. Duan, L. Yuan, H. Zhu, J. Li, Q. Wen, G. I. N. Waterhouse, X. Yang and K. Yan, Polymerization stabilized black-phase FAPbI3 perovskite solar cells retain 100% of initial efficiency over 100 days, *Chem. Eng. J.*, 2021, **419**, 129482.
58 Y. Xu, G. Liu, J. Hu, G. Wang, M. Chen, Y. Chen, M. Li, H. Zhang and Y. Chen, In Situ Polymer Network in Perovskite Solar Cells Enabled Superior Moisture and Thermal Resistance, *J. Phys. Chem. Lett.*, 2022, **13**(16), 3754–3762.
59 A. Farooq, I. M. Hossain, S. Moghadamzadeh, J. A. Schwenzer, T. Abzieher, B. S. Richards, E. Klampaftis and U. W. Paetzold, Spectral Dependence of Degradation under Ultraviolet Light in Perovskite Solar Cells, *ACS Appl. Mater. Interfaces*, 2018, **10**(26), 21985–21990.
60 S.-W. Lee, S. Kim, S. Bae, K. Cho, T. Chung, L. E. Mundt, S. Lee, S. Park, H. Park, M. C. Schubert, S. W. Glunz, Y. Ko, Y. Jun, Y. Kang, H.-S. Lee and D. Kim, UV Degradation and Recovery of Perovskite Solar Cells, *Sci. Rep.*, 2016, **6**(1), 38150.
61 J. Wei, Q. Wang, J. Huo, F. Gao, Z. Gan, Q. Zhao and H. Li, Mechanisms and Suppression of Photoinduced Degradation in Perovskite Solar Cells, *Adv. Energy Mater.*, 2021, **11**(3), 2002326.
62 B. Li, X. Wu, H. Zhang, S. Zhang, Z. Li, D. Gao, C. Zhang, M. Chen, S. Xiao, A. K. Y. Jen, S. Yang and Z. Zhu, Efficient and Stable Tin Perovskite Solar Cells by Pyridine-Functionalized Fullerene with Reduced Interfacial Energy Loss, *Adv. Funct. Mater.*, 2022, **32**(39), 2205870.
63 T. T. Ngo, I. Suarez, G. Antonicelli, D. Cortizo-Lacalle, J. P. Martinez-Pastor, A. Mateo-Alonso and I. Mora-Sero, Enhancement of the Performance of Perovskite Solar Cells, LEDs, and Optical Amplifiers by Anti-Solvent Additive Deposition, *Adv. Mater.*, 2016, 1604056.
64 H. Dong, C. Ran, W. Gao, N. Sun, X. Liu, Y. Xia, Y. Chen and W. Huang, Crystallization Dynamics of Sn-Based Perovskite Thin Films: Toward Efficient and Stable Photovoltaic Devices, *Adv. Energy Mater.*, 2022, **12**(1), 2102213.
65 X. Meng, Y. Li, Y. Qu, H. Chen, N. Jiang, M. Li, D. J. Xue, J. S. Hu, H. Huang and S. Yang, Crystallization Kinetics Modulation of FASnI(3) Films with Pre-nucleation Clusters for Efficient Lead-Free Perovskite Solar Cells, *Angew Chem. Int. Ed. Engl.*, 2021, **60**(7), 3693–3698.
66 W. T. M. Van Gompel, R. Herckens, G. Reekmans, B. Ruttens, J. D'Haen, P. Adriaensens, L. Lutsen and D. Vanderzande, Degradation of the Formamidinium Cation and the Quantification of the Formamidinium–Methylammonium Ratio in Lead Iodide Hybrid Perovskites by Nuclear Magnetic Resonance Spectroscopy, *J. Phys. Chem. C*, 2018, **122**(8), 4117–4124.

67 Y. Su, J. Yang, H. Rao, Y. Zhong, W. Sheng, L. Tan and Y. Chen, Environmentally friendly anti-solvent engineering for high-efficiency tin-based perovskite solar cells, *Energy Environ. Sci.*, 2023, **16**(5), 2177–2186.

68 J. Pascual, S. Collavini, S. F. Völker, N. Phung, E. Palacios-Lidon, L. Irusta, H.-J. Grande, A. Abate, R. Tena-Zaera and J. L. Delgado, Unravelling fullerene–perovskite interactions introduces advanced blend films for performance-improved solar cells, *Sustain. Energy Fuels*, 2019, **3**(10), 2779–2787.

69 K. Nishimura, M. A. Kamarudin, D. Hirotani, K. Hamada, Q. Shen, S. Iikubo, T. Minemoto, K. Yoshino and S. Hayase, Lead-free tin-halide perovskite solar cells with 13% efficiency, *Nano Energy*, 2020, **74**, 104858.

70 T. C. Taucher, I. Hehn, O. T. Hofmann, M. Zharnikov and E. Zojer, Understanding Chemical versus Electrostatic Shifts in X-ray Photoelectron Spectra of Organic Self-Assembled Monolayers, *J. Phys. Chem. C*, 2016, **120**(6), 3428–3437.

71 L. Lanzetta, L. Gregori, L. H. Hernandez, A. Sharma, S. Kern, A. M. Kotowska, A.-H. Emwas, L. Gutiérrez-Arzaluz, D. J. Scurr, M. Piggott, D. Meggiolaro, M. A. Haque, F. De Angelis and D. Baran, Dissociative Host-Dopant Bonding Facilitates Molecular Doping in Halide Perovskites, *ACS Energy Lett.*, 2023, **8**(7), 2858–2867.

72 F. Hao, C. C. Stoumpos, D. H. Cao, R. P. H. Chang and M. G. Kanatzidis, Lead-free solid-state organic–inorganic halide perovskite solar cells, *Nat. Photonics*, 2014, **8**(6), 489–494.

73 G. Zheng, C. Zhu, J. Ma, X. Zhang, G. Tang, R. Li, Y. Chen, L. Li, J. Hu, J. Hong, Q. Chen, X. Gao and H. Zhou, Manipulation of facet orientation in hybrid perovskite polycrystalline films by cation cascade, *Nat. Commun.*, 2018, **9**(1), 2793.

74 S. J. Kim, J. Byun, T. Jeon, H. M. Jin, H. R. Hong and S. O. Kim, Perovskite Light-Emitting Diodes via Laser Crystallization: Systematic Investigation on Grain Size Effects for Device Performance, *ACS Appl. Mater. Interfaces*, 2018, **10**(3), 2490–2495.

75 Z. Zhang, L. Wang, A. Kumar Baranwal, S. Razey Sahamir, G. Kapil, Y. Sanehira, M. Akmal Kamarudin, K. Nishimura, C. Ding, D. Liu, Y. Li, H. Li, M. Chen, Q. Shen, T. S. Ripolles, J. Bisquert and S. Hayase, Enhanced efficiency and stability in Sn-based perovskite solar cells by trimethylsilyl halide surface passivation, *J. Energy Chem.*, 2022, **71**, 604–611.

76 E. V. Péan, S. Dimitrov, C. S. De Castro and M. L. Davies, Interpreting time-resolved photoluminescence of perovskite materials, *Phys. Chem. Chem. Phys.*, 2020, **22**(48), 28345–28358.

77 K. T. Cho, S. Paek, G. Grancini, C. Roldán-Carmona, P. Gao, Y. Lee and M. K. Nazeeruddin, Highly efficient perovskite solar cells with a compositionally engineered perovskite/hole transporting material interface, *Energy Environ. Sci.*, 2017, **10**(2), 621–627.

78 H. J. Snaith, A. Abate, J. M. Ball, G. E. Eperon, T. Leijtens, N. K. Noel, S. D. Stranks, J. T.-W. Wang, K. Wojciechowski and W. Zhang, Anomalous Hysteresis in Perovskite Solar Cells, *J. Phys. Chem. Lett.*, 2014, **5**(9), 1511–1515.

79 A. Kumar, J. Mahato, M. Dixit and G. N. Patwari, Progressive Hydrophobicity of Fluorobenzenes, *J. Phys. Chem. B*, 2019, **123**(47), 10083–10088.

80 S. Valero, T. Soria, N. Marinova and J. L. Delgado, Efficient and stable perovskite solar cells based on perfluorinated polymers, *Polym. Chem.*, 2019, **10**(42), 5726–5736.